Monolayer hexagonal arsenene with tunable electronic structures and magnetic properties *via* impurity doping

Zhongjun Li,[a] Wei Xu,[a] Yuanqin Yu,[b] Hongyang Du,[a] Kun Zhen,[a] Jun Wang,[a] Linbao Luo,*[a] Huaili Qiu[a] and Xiaobao Yang*[c]

[a] School of Electronic Science and Applied Physics, Hefei University of Technology, Hefei, Anhui 230009, China

[b] School of Physics and Material Science, Anhui University, Hefei, Anhui 230039, China

[c] Department of Physics, South China University of Technology, Guangzhou, Guangdong 510641, China

Abstract

Monolayer hexagonal arsenene (hAs), a typical two-dimensional semiconducting material with a wide band gap and high stability, has attracted increasing research interest due to its potential applications in optoelectronics. Using first-principles calculations, we have investigated the electronic and magnetic properties of x-substituted hAs (x = B, C, N, O, Ga, Ge, Se, and monovacancy) and x-adsorbed hAs (x = As). Our results show that the B-, N-, and Ga-substituted hAs have spin-unpolarized semiconducting characters like pristine hAs, and the indirect-direct band gap transitions are induced in the B- and N-substituted systems. In contrast, the O-, Se-, and monovacancy-substituted hAs are metallic, and the C- and Ge-substituted hAs show spin-polarization semiconducting characters with the band gaps of 1.1 and 1.3 eV for the spin-up channels and 1.0 and 0.7 eV for the spin-down channels, respectively. For the As-adsorbed hAs, the Fermi level crosses the spin-up states, yielding metallic behavior, while the spin-down channel remains semiconducting character. The detailed analysis of electronic structures for the C-substituted, Ge-substituted, and As-adsorbed hAs shows that the strong hybridizations between the doping atoms and As atoms lead to the energy splitting near Fermi level and consequently induce magnetic moments. By selective doping, hAs can be transformed from spin-nonpolarized semiconductor, to spin-polarized semiconductor, to half-metal, and even to metal, which indicates that the doped hAs will have promising potential in future electronics, spintronics, and optoelectronics.

Keywords: monolayer hexagonal arsenene; 2-D materials; doping; half-metal; first-principles calculation

1. Introduction

Due to the integration limit of silicon-based devices, more and more attentions have been paid to two-dimensional (2D) materials, such as graphene,[1, 2] silicene,[3, 4] boron nitride,[5-7] transition metal dichalcogenides,[8-10] and black phosphorus,[11-13] due to their rather unique properties. The atomic level thickness of these materials leads to substantially novel performances in electronic structures. For example, a transition of indirect-direct band gaps occurs when MoS_2 changes from multilayer or bulk to monolayer one.[9] Furthermore, the devices based on these 2D materials show small short channel effects and excellent electrostatic modulations because of their ultrathin thickness. Therefore, in recent years, many high-performance electronic and optoelectronic devices based on these 2D materials have been developed.[10-17]

Recently, two studies on 2D arsenene sheet were performed by first-principles calculations. Zhang et al. predicted two types of 2D materials, monolayer hexagonal arsenene (hAs) and antimonene (hSb), which exhibit typical semiconducting characteristics with high stability and wide indirect band gaps of 2.49 and 2.28 eV, respectively.[18, 19] Moreover, under small biaxial strain, these two materials were found to transform from indirect into direct band gap.[18] Kamal et al. systematically investigated the stability and electronic properties of arsenic system, including buckled and puckered honeycomb structures, both of which possess indirect gaps and undergo an indirect-to-direct band gap transition by applying strain.[19] Such essential changes in electronic structures will facilitate the fabrications of transistors with high on/off ratio, optoelectronic devices, and mechanical sensors.[18, 19]

Due to the potential applications, more recently, several theoretical studies on hAs and its analogs have been performed in an effort to tune their electronic properties.[20-24] For example, Kou et al studied the geometric structures, electronic properties, and external strain deformation effect of hAs and antimony arsenide.[20] It was revealed that both materials are indirect band semiconductors, and an indirect-direct band gap transition can be achieved when small tensile strain is applied.[20] On the basis of first-principles calculations, Wang et al found that for hAs and hSb sheet, the armchair nanoribbons are indirect semiconductors while the zigzag nanoribbons are direct ones regardless of the ribbon width.[21]

It is noted that, despite of the huge progresses mentioned above, the means to tune electronic structures of hAs and hSb are limited to exerting external strain on the sheets or cutting them into nanoribbons, which are difficult in practice. As is known, doping is a feasible method for modifying electronic and magnetic properties of semiconducting materials, such as MoS_2,[25-27] hBN,[28-30] germanium,[31, 32] and so on. It

is recognized that practically stable doping requires substitution of host atoms, where the doping is secured through covalent bonding. For hAs and hSb sheets, doping is highly desirable as the tailoring of electrical property is paramount to their devices application. Therefore, considering the larger band gap in hAs than that in hSb sheet, we have theoretically investigated the possibility to tune electronic structures and magnetic properties of hAs by substitutional doping with various atoms of B, C, N, O, Ga, Ge, and Se. In addition, the doping of monovacancy and adsorption of As atom have also been investigated because these two types of impurities may occur in the preparation of hAs.

In the present work, the structural stabilities, electronic structures, and magnetic properties of x-substituted hAs (x = B, C, N, O, Ga, Ge, Se, and monovacancy) and x-adsorbed hAs (x = As) have systematically been studied based on first-principle calculations. The influences of doping on geometric structures are evaluated by comparison of structural parameters for the systems before/after doping. On the basis of the optimized geometric structures, formation energies, magnetic moments, and charge transfers from doping atoms to hAs are obtained. For all doped systems, the conducting characteristics are emphatically studied on the basis of the spin-polarized band structures and partial density of states (PDOS). This work will explore the possibility of tuning the electronic properties of arsenene sheets, as well as other 2D systems, by proper atomic doping.

2. Computational methods

The first-principles calculations were performed based on density functional theory (DFT) implemented in the Vienna ab initio simulation package (VASP).[33-35] The exchange correlation potential was approximated by the generalized gradient approximation (GGA) with PBE functional.[36] Electronic wave functions were expanded using a plane-wave basis set with a cutoff energy of 550 eV. A 4×4 supercell consisting of 16-fold unit cells of hAs was used with a vacuum space of 15 Å to eliminate the cell-to-cell interactions. One B, C, O, Ga, Ge, and Se atom was used to substitute one As atom in the supercell, respectively. Moreover, the monovacancy and the adsorption of an isolated As atom were also considered in the supercell, respectively. The impurity concentration is 1/32. The test calculation was also carried out for 6×6 supercell with a smaller concentration, and the main results, as shown in Fig. S1 in electronic supplementary information (ESI), keep unchanged. Therefore, all the theoretical simulations were carried out with the 4×4 supercell. The Monkhorst-Pack k-point samplings in Brillouin zone are 7×7×1 and 13×13×1 meshes

in the optimization of geometrical structures and the calculation of electronic structures, respectively. The full-relaxation of structures with spin-nonpolarization and spin-polarization calculations were carried out until the force components were smaller than 0.01 eV/Å, and the convergence criteria is 10^{-4} eV for energy. Bader analysis was used to calculate the charge transfer.[37] To evaluate the stability of the doped systems, the formation energy is defined as $E_f = E_{complex} + E_{As} - (E_{hAs} + E_x)$, where $E_{complex}$ and E_{hAs} are the total energies of the doped and pristine hAs systems, and E_{As} and E_x are the energies of the atoms in its bulk form except for the cases, in which the energies of x atoms (x = N and O) in its molecular gas phase are employed. By including the spin-orbit coupling effects in the calculations, we found that these effects on band structures of the doped systems can be neglected, as shown in Fig. S2 and S3 (ESI). Therefore, the spin-orbit coupling effects are not included in the following calculations.

Table 1 Typical geometrical parameters, formation energy (E_f), charge transfer (Δq), and magnetic moment (M) for x-substituted hAs (x = B, C, N, O, Ga, Ge, Se, and monovacancy) and x-absorbed hAs (x = As).

	$d_{x\text{-}As1}$ (Å)	$d_{As1\text{-}As4}$ (Å)	h (Å)	E_f (eV)	Δq (e)	M (μ_B)
B-substituted hAs	1.97	2.48	0.71	4.67	0.05	0.0
C-substituted hAs	1.99	2.49	0.82	6.46	0.99	1.0
N-substituted hAs	2.01	2.50	1.34	0.34	1.15	0.0
O-substituted hAs	2.02	2.47	1.11	0.64	0.98	0.0
Ga-substituted hAs	2.43	2.49	1.19	4.02	–0.49	0.0
Ge-substituted hAs	2.48	2.46	1.22	4.64	–0.31	1.0
Pristine hAs	2.51	2.51	1.39	--	--	0.0
Se-substituted hAs	2.52	2.46	1.38	4.07	0.27	0.0
Monovacancy-substituted hAs	--	2.47	--	5.04	--	0.0
As-adsorbed hAs	2.69	2.61	1.82	2.64	0.09	3.0

3. Results and discussion

3.1 x-substituted hAs (x = B, C, N, O, Ga, Ge, and Se atoms)

Relative energy of the electronic states with different magnetic moments for pristine hAs and x-substituted hAs (x= B, C, N, O, Ga, Ge, and Se atoms) were listed in Table S1 (ESI). From the table one can see that only the C- and Ge-substituted hAs in the ground states have magnetic moment of 1.0 μ_B, while other doped systems, especially the O- and Se-substituted hAs, possess the ground states with zero magnetic moment.

For these ground states, typical geometric parameters, formation energy, and charge transfer were calculated and summarized in Table 1. The positive values of formation energies indicate that the formation process of the doped systems is endothermic. Moreover, the values are determined not only by the doped systems, but also by material states of the doping atoms. In particular, for the x-substituted hAs (x = N and O atoms), the formation energies are obviously smaller than other systems due to the small energies of x atoms in its molecular gas phase. For the pristine hAs, the As–As bond length and the height of buckling layer are predicted to be ~ 2.51 and 1.39 Å, respectively, in agreement with the values of 2.55 and 1.35 Å calculated by Zhang et al. with the GGA/PBE functional.[18] When one As atom in the pristine hAs is substituted by x atoms, the x–As1 bonds (x = B, C, N, O, Ga, Ge, and Se), as shown in Fig. 1, are predicted to be shorter than the As–As bonds of the pristine hAs. Notably, much shorter x–As1 bonds occur in the x-substituted hAs (x = B, C, N, and O) due to small atomic radius and strong electronegativity of substitutional atoms. Because of the substitutional effect, the As1–As4 bonds in all x-substituted hAs are a little bit longer than that of the As–As bonds in hAs. Moreover, compared with that between two layers of As atoms in the pristine hAs, the distances between the substitutional atoms and the bottom layer of As atoms clearly become shorter in all x-substituted hAs except for the N-substituted hAs, in which an equivalent distance to the pristine hAs are observed. These equivalent distances should be attributed to the similar hybridization characters between N and As atoms, which facilitate to form buckling structures.

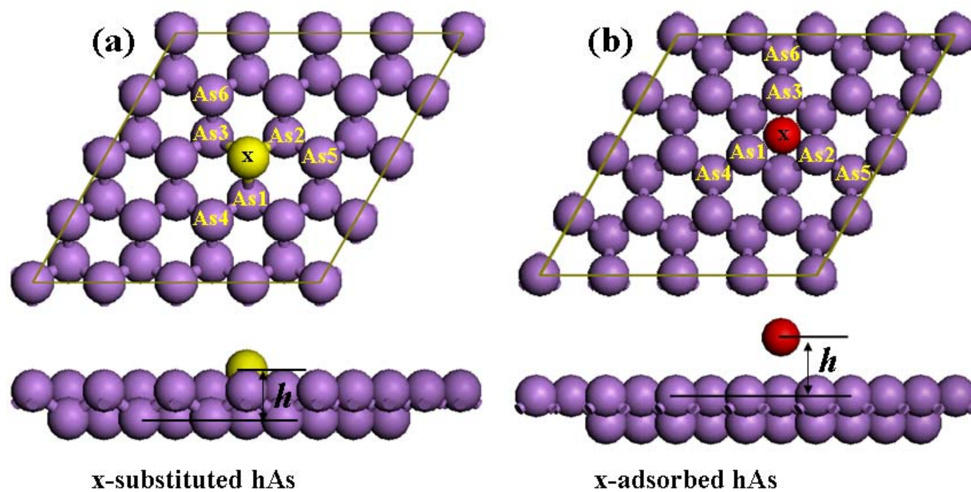

Fig. 1 Top and side views of (a) x-substituted hAs (x = B, C, N, O, Ga, Ge, Se, and monovacancy) and (b) x-absorbed hAs (x = As). For clarify, the near-neighbor As atoms of the dopants x atoms are labeled, and other balls present As atoms in each

graph.

Based on the Bader analysis, charge transfer from the substitutional atoms to the monovacancy-hAs is also examined. Compared with the isolated atoms, the electron accumulations about 0.05*e*, 0.99*e*, 1.15*e*, 0.98*e*, and 0.27*e* occur at the B, C, N, O and Se atoms, whereas the electron depletions are about 0.49*e* and 0.31*e* at the Ga and Ge atoms of the doped hAs, respectively. The electron accumulations and depletions reflect the relative differences in electronegativity of B, C, N, O, Ga, Ge, As, and Se atoms from As atom. On the other hand, the obvious charge transfers indicate the essential bonding between the substitutional atoms and the As atoms, showing the stability of the doped hAs.

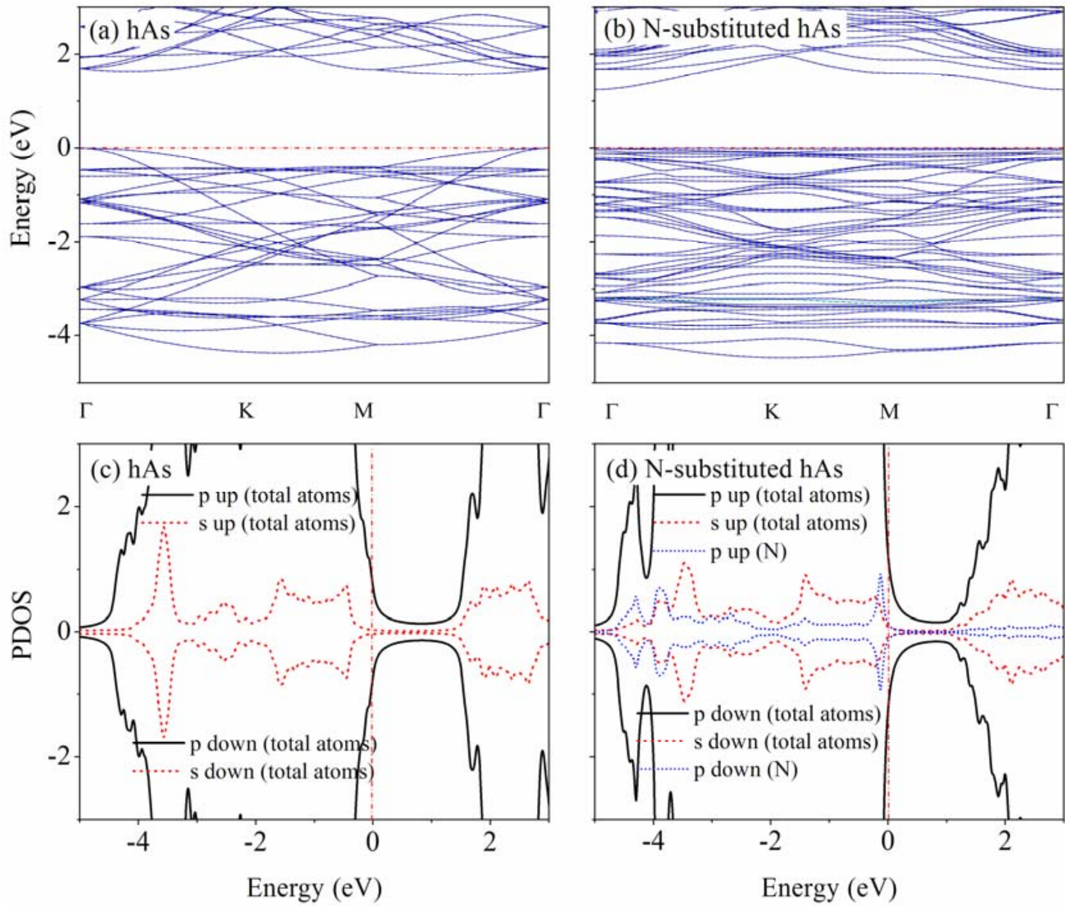

Fig. 2 Spin-polarized band structures and PDOS of the pristine and the N-substituted hAs. Black solid and blue dashed lines in band structures denote spin-up and spin-down channels, respectively. Red dash-dot lines indicate the Fermi level in band structures and PDOS. To clearly show the delicate contributions from the substitutional atoms near Fermi level, the range of ordinate in (c) and (d) was set from -3 to 3 eV, and the DOS of total atoms lies partially outside the range.

The spin-polarized band structures and PDOS of the pristine and the N-substituted hAs were presented in Fig. 2. For the pristine hAs sheet, the band structures for up and down spins are the same, as shown in Fig. 2(a), leading to zero magnetic moment. The indirect band gap is estimated to be about 1.6 eV, which is generally consistent with the one calculated by Zhang et al with the GGA/PBE functional.[18]. It is clear that the band gap calculated by the GGA/PBE functional is smaller than that calculated by using HSE06, as shown in Fig. S4 (ESI). This difference in band gap should be attributed to the fact that GGA/PBE functional usually overestimates electron delocalization, leading to smaller band gap, while HSE06 may correct this overestimation by partially including Hartree-Fock (HF) functional, which is known to localize electrons. Remarkably, when one As atom is substituted by one N atom, as shown in Fig. 2(b), the indirect band gap will transform into a direct band gap of 1.3 eV at the Γ point in Brillouin zone, remaining the spin-unpolarized characteristics. In order to further understand the origin of the valence band (VB) and the conduction band (CB), the spin-polarized PDOS of the pristine and N-substituted hAs sheets were presented in Fig. 2(c) and (d), respectively. It is shown that the VB and CB of pristine hAs have similar components, i.e., the 4p states coupled with small amounts of the 4s states of As atoms. When one N atom is introduced to substitute an As atom in the supercell of the pristine hAs, no dangling bond appears in the three nearest-neighbor As atoms and no impurity gap states occur in the band gap, which is understandable as the N and As atoms belong to the same family of V group in the Periodic Table and have the similar hybridized characters.

When one As atoms in the pristine hAs is substituted by one x atom (x = B, C, O, Ga, Ge, and Se), obvious impurity gap states occur in the band structures of the x-substituted hAs, as shown in Fig. 3. One can clearly see that similar to the pristine hAs, the B-, Ga-, O-, and Se-substituted hAs are all spin-unpolarized. Nevertheless, when C and Ge atoms are introduced to substitute As atoms, the resultant hAs exhibit typical spin-polarized character. In the B-substituted hAs, the substitutional effect can induce three impurity gap states. One state is occupied appearing above the VB maximum about 0.1 eV, while another two are unoccupied occurring below the CB minimum about 0.40 eV. The direct band gap about 1.35 eV is observed. In the Ga-substituted hAs, the similar electronic structures to the B-substituted system are observed except for an indirect band gap about 1.25 eV. In the C-substituted hAs, two impurity gap states appear above the VB maximum about 0.52 and 1.13 eV, respectively, as shown in Fig. 3(c). Similar two impurity gap states occur above the

VB maximum about 0.45 eV and below the CB minimum about 1.15 eV in the Ge-substituted hAs, as shown in Fig. 3(d). It should be noted that for both C- and Ge-substituted systems, the two gap states belong to the up- and down-spin components, respectively. One is occupied and the other is unoccupied, and the Fermi level is located in the gap between these two gap states. The detailed conducting characters of both C- and Ge-substituted hAs sheets will be analyzed according to the PDOS in Fig. 4. Interestingly, when one As atom in the pristine hAs is respectively substituted by one O or one Se atom, as shown in Fig. 3(e) and (f), obvious impurity states crossing Fermi level are observed, indicative of the metallic characters for both doped systems.

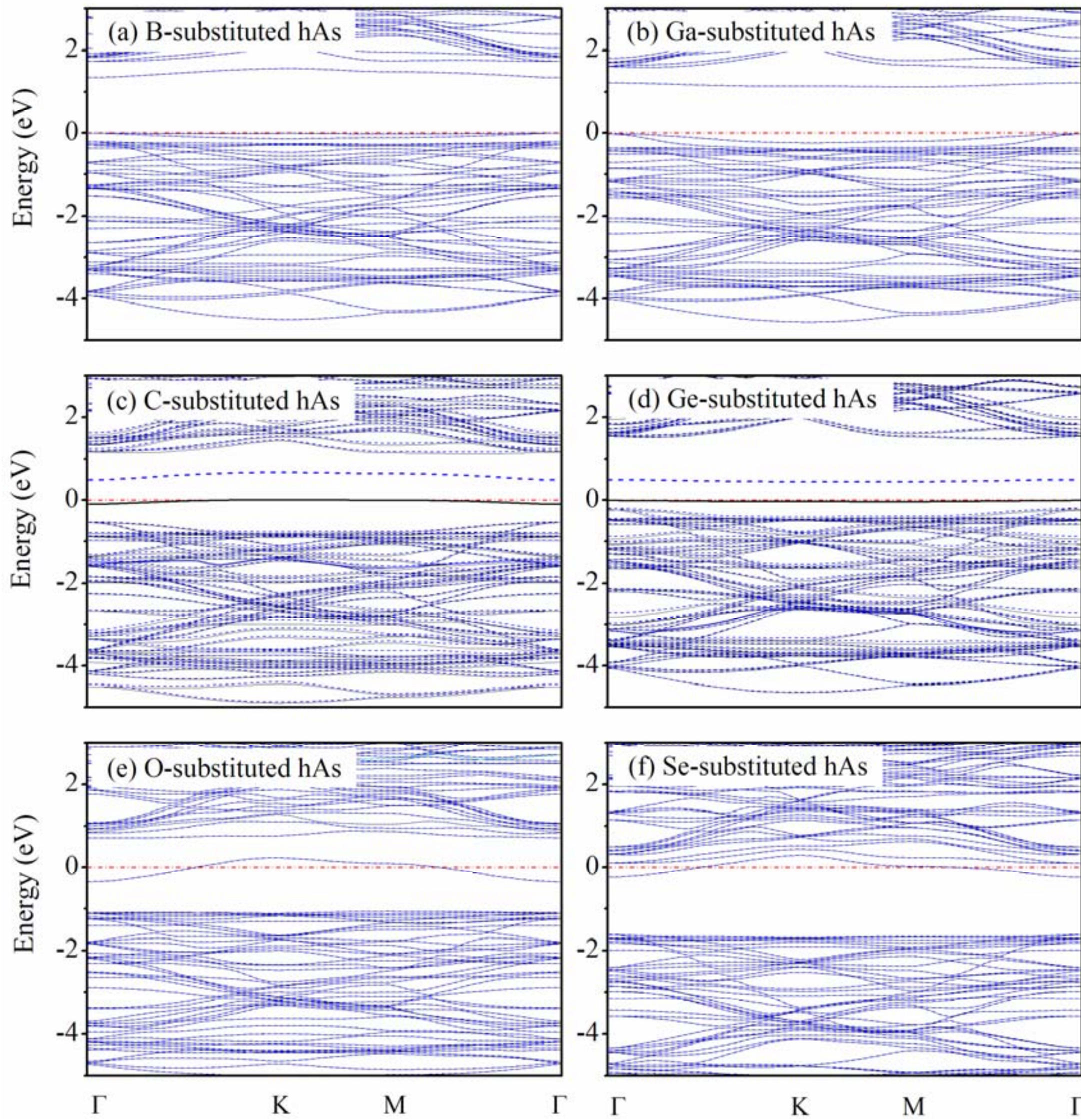

Fig. 3 Spin-polarized band structures of (a) B-substituted, (b) Ga-substituted, (c) C-substituted, (d) Ge-substituted, (e) O-substituted, and (f) Se-substituted hAs. Black solid and blue dashed lines denote spin-up and spin-down channels and red dash-dot

lines indicate the Fermi level, respectively.

The components of the VB, CB, and impurity gap states and the magnetic properties of the x-substituted hAs (x = B, Ga, C, Ge, O, and Se) are uncovered by the spin-polarized PDOS presented in Fig. 4. It is shown that the VB and CB of the doped systems are primarily composed of the 4p states of As atoms, and the origin of the corresponding impurity gap states are generally complicated. As shown in Fig. 4(a), in the B-substituted hAs, the two occupied gap states consist of the 4p states of the three nearest-neighbor atoms of As1, As2, and As3, whereas the unoccupied gap states are primarily contributed from the 2p states of B atom coupled with small amount of the 4p states of the three nearest-neighbor As1, As2, and As3 atoms. These impurity states decrease the band gaps. Similar cases are also observed in Fig. 4(b) for the Ga-substituted hAs. Since the hybridizations between the substitutional atoms and the As atoms are very weak, these two doped systems keep spin-unpolarized characters.

The PDOS in Fig. 4(c) and (d) show that in the impurity gap state of the C- and Ge-substituted hAs, there are almost equivalent contributions from the 2p states of the C atom and the 4p states of the three nearest-neighbor atoms of As1, As2, and As3, indicating strong orbital hybridizations between the C atom and its nearest-neighbor As atoms. Unlike the B-, N-, and Ga-substituted hAs, the strong hybridizations cause the splitting of the bands between the spin-up and spin-down channels near Fermi level in the impurity gap state of the C- and Ge-substituted hAs. Due to these splitting, the C- and Ge-substituted hAs exhibits spin-polarized semiconducting characters with the band gaps of 1.1 and 1.3 eV for the spin-up channels, and with the band gaps of 1.0 and 0.7 eV for the spin-down channels, respectively. Moreover, for these two doped systems, the band gaps between the spin-up VB and spin-down CB are 0.35 and 0.25 eV, respectively. The splitting between spin-up and spin-down channels induces magnetic moments of 1.0 μ_B in the C- and Ge-substituted hAs, as shown by data in Table 1. To further understand the origin of the magnetic moments, the spin densities were calculated for the C- and Ge-substituted hAs. For simplicity, only spin density image for the C-substituted hAs is presented in Fig. 5(a). One can see that the spin density is mainly localized at the substitutional C atom and their nearest-neighbor As atoms, consistent to the observation in the PDOS presented in Fig. 4(c).

For the metallic O-substituted hAs with an impurity gap state crossing Fermi level, its gap states are dominated by the 4p states of the three nearest-neighbor atoms of As1, As2, and As3, and the contribution from the substitutional O atom is too small to be negligible, as shown in Fig. 4(e). Therefore, the O-substituted hAs exhibits spin-unpolarized metallicity, different from the C- and Ge-substituted systems with

net magnetic moment of 1.0 μ_B. Although no obvious impurity gap state occurs in the Se-substituted hAs, the Fermi level crosses the CB minimum, and the doped system is thus metallic as well with spin-unpolarized character, as shown in Fig. 4(f). To further give some insight into the spin-unpolarized character of O- and Se-substituted hAs, we compared their PDOS with those of the C- and Ge-substituted systems. It can be seen from Fig. 4(c–f) that in the O- and Se-substituted hAs the *p* electrons of O and Se atoms are more delocalized than those of the C- and Ge-substituted systems, especially near the Fermi level. Therefore, in view of the poor hybridization between the substituted atoms of O and Se and the three nearest-neighbor As atoms, the O- and Se-substituted hAs should have zero magnetic moments.

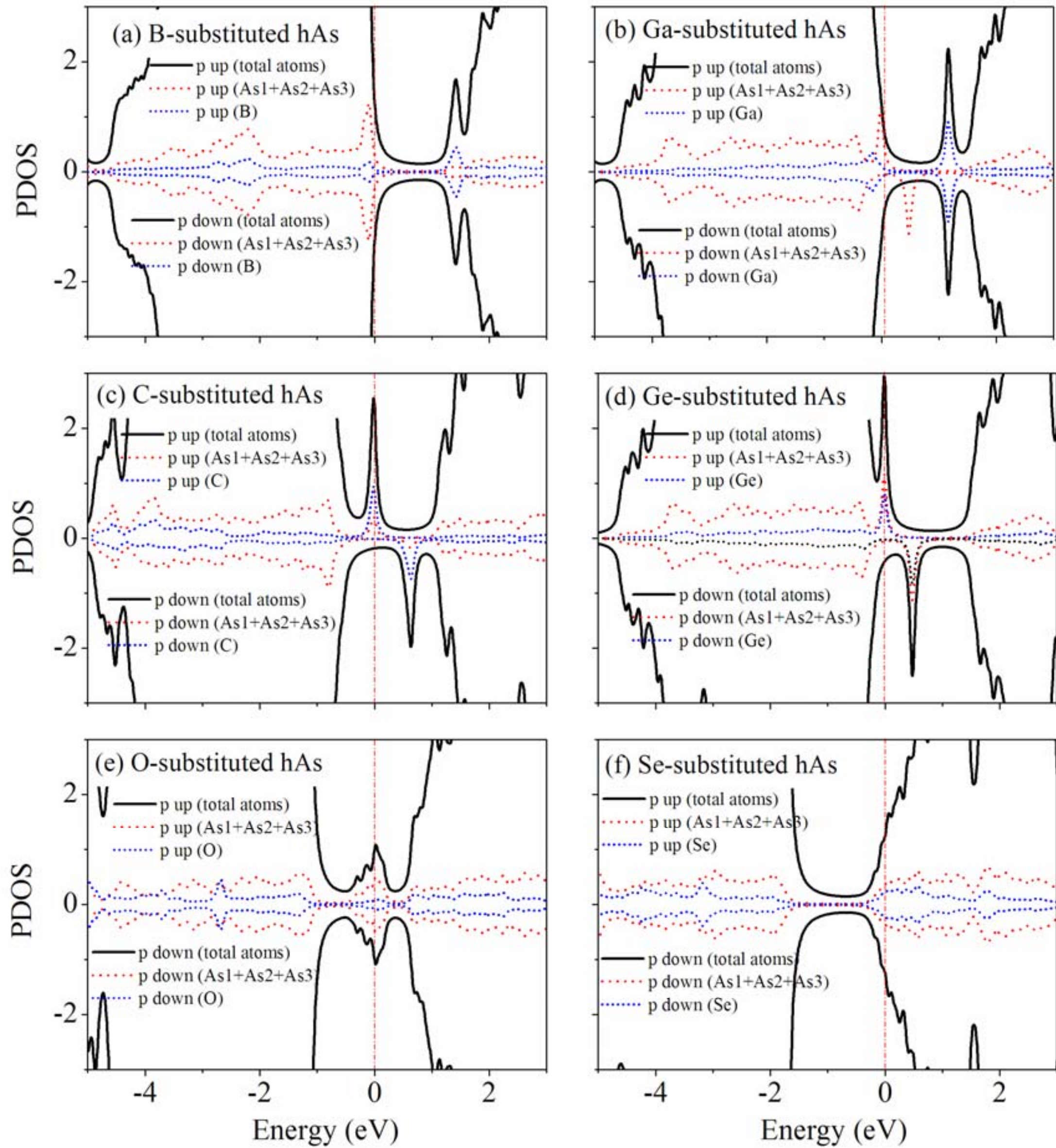

Fig. 4 Spin-polarized PDOS of (a) B-substituted, (b) Ga-substituted, (c) C-substituted,

(d) Ge-substituted, (e) O-substituted, and (f) Se-substituted hAs. Red dash-dot lines indicate the Fermi level. To clearly show the delicate contributions from the substitutional atoms near Fermi level, the ranges of ordinates were set from -3 to 3 eV, and the DOS of total atoms lies partially outside the range.

From above discussion one can see that, in general, the doped hAs, in which the doping atoms belong to the same group in the Periodic Table, show virtually similar electronic structures and magnetic property due to their similar electronic structures. However, they can have different geometrical parameters, formation energies, charge transfer mainly due to different atomic radiuses and electronegativity. What is more, for the doped systems, in which the doping atoms belong to the different groups, the obviously different properties were observed. For example, it is expected that the B- and Ga-substituted hAs with even electrons are spin-unpolarized and the C- and Ge-substituted hAs with odd electrons have typical spin-polarized characteristics with magnetic moment of 1.0 μ_B. However, spin-unpolarized characteristics were observed in the O- and Se-substituted systems with odd electrons due to the delocalizations of *p* electrons in doping atoms of O and Se.

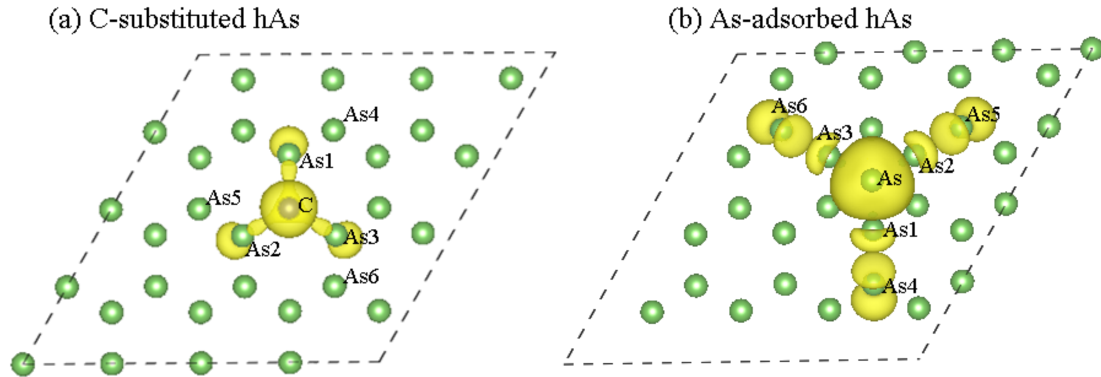

Fig. 5 Spin density image for (a) C-substituted (b) As-adsorbed hAs. The substitutional C, the adsorbed As, and their near-neighbor As atoms are labeled, and other balls present As atoms without special label.

3.2 Monovacancy-substituted and As-adsorbed hAs

Besides the atom-substituted doping, the influence of vacancy and adsorption of As atom on electronic structures of hAs was also investigated since these two types of impurities may occur in the preparation of hAs. There is one configuration for the monovacancy-substituted doping in the supercell. For the adsorption of As atom on surface of the pristine hAs, two configurations are considered. One is the top

configuration in which the adsorbed As atom is on top site of As atom, the other is the hollow configuration in which the As atom is on hollow site of pristine hAs. The total energy calculations indicate that the hollow configuration is more stable. Thus only this configuration, as shown in Fig. 1(b), is further studied.

For the monovacancy-substituted and the As-absorbed hAs, the geometric parameters, formation energy, and charge transfer were presented in Table 1. The formation energies calculated indicate that the formation of the monovacancy-substituted and As-absorbed hAs is an endothermic process. In the monovacancy-substituted hAs, the As1–As4 bond becomes shorter than that in the pristine hAs. To evaluate the strength of the bond between the adsorbed As atom and hAs sheet, the adsorption energy was calculated by the formula $E_a = E_{complex} - (E_{hAs} + E_x)$, where $E_{complex}$ and E_{hAs} are the total energies of As-absorbed hAs and pristine hAs sheets, and E_x is the energy of isolated As atom, respectively. The calculated adsorption energy of –0.34 eV indicates that As atom can be chemically adsorbed on the hAs sheet. What is more, the distance between the absorbed atom of As and the top As layer of hAs is about 1.82 Å, and the length of the As–As1 bond is about 2.69 Å, further indicating chemical bonding interaction between the adsorbed As atom and the As1, As2, and As3 atoms, respectively. In fact, these chemical bonding was further confirmed by Bader charge analysis, which reveals electron accumulation about 0.09*e* at the absorbed As atom. Detailed discussion of the bonding interaction will be entertained afterwards.

The spin-polarized band structures and the PDOS of the monovacancy-substituted and As-adsorbed hAs are presented in Fig. 6. One can see from Fig. 6(a) that the band structures of up- and down-spin components are virtually identical. Two impurity gap states are induced by the monovacancy substitution. One is partially occupied and the other is unoccupied, and the doped system is metallic. The symmetry of PDOS in the spin-up and spin-down channels in Fig. 6(c) shows that the gap states are mainly contributed from the 4p states of the three nearest-neighbor As1, As2, and As3 atoms. In view of the absence of one As atom, the nature of these gap states should be associated with the dangling bonds of the As1, As2, and As3 atoms.

In contrast, the adsorption of an As atom on the surface of the pristine hAs causes the formation of six impurity gap states, as shown in Fig. 6(b). One state is occupied, two are partially occupied, and the other three are unoccupied. The former three states belong to the spin-up components and the latter three are spin-down ones. The PDOS in Fig. 6(d) indicates that on the one hand, the energy level splits near the Fermi level between the spin-up and spin-down channels. The spin-up component crosses the

Fermi level and yields metallic character while the spin-down channel remains semiconducting. The energy splitting near the Fermi level induces a magnetic moment about 3.0 μ_B, as listed in Table 1. In light of this, the As-adsorbed hAs is half-metallic. On the other hand, the PDOS in Fig. 6(d) shows that the origin of these impurity gap states is mainly the hybridization of the 4p states of the adsorbed As atoms and those of the next-nearest-neighbor atoms of As4, As5, and As6, as labeled in Fig. 1(b). In comparison, the contributions from the 4p states of three nearest-neighbor As1, As2, and As3 atoms are slight. Therefore, the magnetic moment can be attributed to the contribution from the hybridization between the 4p states of the adsorbed As atoms and its next-nearest-neighbor As atoms. These results are unexpected and interesting because the adsorbed As atom are bonded not directly with the As4, As5, and As6 atoms, but with the three nearest-neighbor atoms of As1, As2, and As3.

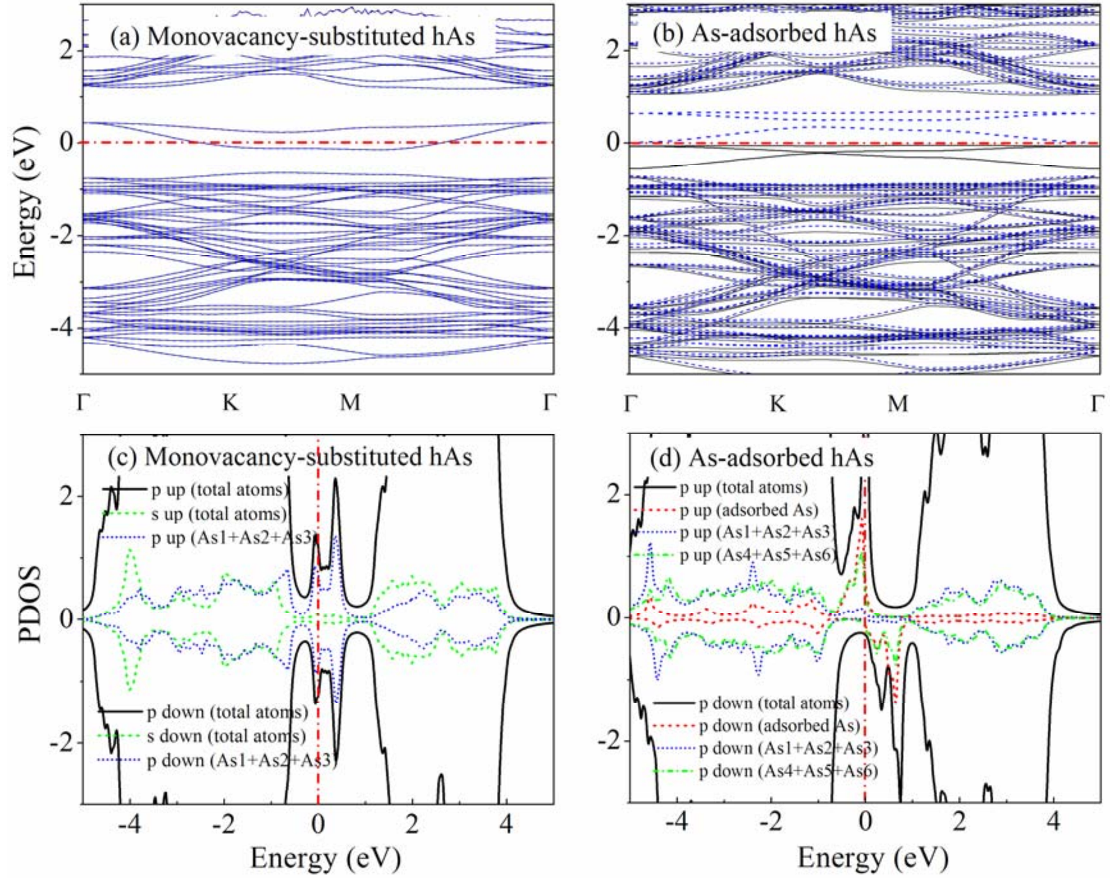

Fig. 6 Spin-polarized band structures and PDOS of the monovacancy-substituted and As-adsorbed hAs. Black solid and blue dashed lines in band structures denote spin-up and spin-down channels, respectively. Red dash-dot lines indicate the Fermi level in band structures and PDOS. To clearly show the delicate contributions from the substitutional atoms near Fermi level, the ranges of ordinates were all set from -3 to 3

eV, and the DOS of total atoms lies partially outside the range.

To further understand the above unexpected results in the As-adsorbed hAs, the bonding characters are analyzed on the basis of the spin density image, as shown in Fig. 5(b). According to the PDOS in Fig. 6(d), the spin polarization only occurs near the Fermi level, thus the spin electron density distributions can reflect the contributions of different atoms to the impurity gap states. It can be seen from Fig. 5(b) that the spin density is mainly localized at the adsorbed As atom and its next-nearest-neighboring atoms of As4, As5 and A6, whereas those at the three nearest-neighbor atoms of As1, As2 and As3 are too small. This observation is consistent with the results observed in the PDOS. On the other hand, the distance of 2.69 Å and the electron accumulations about 0.09*e* on the adsorbed As atom indicate the essential bonding between the adsorbed As atom and the three nearest-neighbor atoms of As1, As2, and As3, as listed in Table 1. Because the bonding between the adsorbed As atom and its nearest-neighbor As1, As2, and As3 atoms lie on the same lines with the As1–As4, As2–As5, and As3–As6 bonds, these bonding interactions consequentially weaken the latter three bonds. As a result, the corresponding bond lengths consequently become larger than the one in the pristine hAs, as indicated by data in Table 1. Understandably, due to the weakened As1–As4, As2–As5, and As3–As6 bonds, the charge distributions in the As4, As5, and As6 atoms become localized toward Fermi level, leading to the metallic behavior of the As-adsorbed hAs.[16]

4. CONCLUSSIONS

In summary, we have theoretically investigated on the electronic and magnetic properties of x-substituted hAs (x = B, C, N, O, Ga, Ge, Se, and monovacancy) and x-adsorbed hAs (x = As) have been reported. The B-, N-, and Ga-substituted hAs keep similar semiconducting characters to pristine hA except for the transition from indirect to direct band gaps in the former two doped systems due to the influences of the impurity gap states. In contrast, the O-, Se-, and monovacancy-substituted hAs sheets exhibits typical metallic behavior, and the C- and Ge-substituted hAs show spin-polarization semiconducting character with the band gaps of 1.1 and 1.3 eV for the spin-up channels and 1.0 and 0.7 eV for the spin-down channels, respectively. For the As-adsorbed hAs, the Fermi level crosses the spin-up states, yielding metallic character, while the spin-down channel remains semiconducting. For the spin-polarized systems, the further analysis of electronic structures indicates that the

hybridization between the doping atoms and the As atoms results in the energy splitting near the Fermi level and consequently induces magnetic moments. We have explicitly demonstrated that the conducting characters of hAs can be easily tuned from spin-nonpolarized semiconductor, to spin-polarized semiconductor, to metal, and to half-metal by selective impurity doping, suggesting its promising applications in future electronics, spintronics, and optoelectronics.

Acknowledgement

This work was supported by the Natural Science Foundation of China (NSFC, Nos. 61575059, 21101051, 11474100), the Anhui Provincial Natural Science Foundation (No. 1408085MA18), the Fundamental Research Funds for the Central Universities (2012HGCX0003, 2013HGCH0012, 2014HGCH0005, JZ2015HGXJ0184, 2015PT017), and the Key Research Foundation of Anhui Provincial Educational Committee (KJ2015A040).

References

1 K. S. Novoselov, A. K. Geim, S. V. Morozov, D. Jiang, Y. Zhang, S. V. Dubonos, I. V. Grigorieva and A. A. Firsov, *Science*, 2004, **306**, 666-669.

2 K. S. Novoselov, A. K. Geim, S. V. Morozov, D. Jiang, M. I. Katsnelson, I. V. Grigorieva, S. V. Dubonos and A. A. Firsov, *Nature*, 2005, **438**, 197-200.

3 P. Vogt, P. De Padova, C. Quaresima, J. Avila, E. Frantzeskakis, M. C. Asensio, A. Resta, B. Ealet and G. Le Lay, *Phys. Rev. Lett.*, 2012, **108**, 155501.

4 G. G. Guzman-Verri and L. C. L. Y. Voon, *Phys. Rev. B*, 2007, **76**, 075131.

5 C. H. Jin, F. Lin, K. Suenaga and S. Iijima, *Phys. Rev. Lett.*, 2009, **102**, 195505.

6 J. C. Meyer, A. Chuvilin, G. Algara-Siller, J. Biskupek and U. Kaiser, *Nano Lett.*, 2009, **9**, 2683-2689.

7 L. Song, L. Ci, H. Lu, P. B. Sorokin, C. Jin, J. Ni, A. G. Kvashnin, D. G. Kvashnin, J. Lou, B. I. Yakobson and P. M. Ajayan, *Nano Lett.*, 2010, **10**, 3209-3215.

8 K. K. Liu, W. J. Zhang, Y. H. Lee, Y. C. Lin, M. T. Chang, C. Su, C. S. Chang, H. Li, Y. M. Shi, H. Zhang, C. S. Lai and L. J. Li, *Nano Lett.*, 2012, **12**, 1538-1544.

9 Y. Zhang, T. R. Chang, B. Zhou, Y. T. Cui, H. Yan, Z. K. Liu, F. Schmitt, J. Lee, R. Moore, Y. L. Chen, H. Lin, H. T. Jeng, S. K. Mo, Z. Hussain, A. Bansil and Z. X. Shen, *Nat. Nanotechnol.*, 2014, **9**, 111-115.

10 X. Huang, Z. Y. Zeng and H. Zhang, *Chem. Soc. Rev.*, 2013, **42**, 1934-1946.

11 H. Liu, Y. C. Du, Y. X. Deng and P. D. Ye, *Chem. Soc. Rev.*, 2015, **44**, 2732-2743.

12 J. Na, Y. T. Lee, J. A. Lim, D. K. Hwang, G. T. Kim, W. K. Choi and Y. W. Song, *ACS Nano*, 2014, **8**, 11753-11762.

13 D. Cakir, H. Sahin and F. M. Peeters, *Phys. Rev. B*, 2014, **90**, 205421.

14 B. Radisavljevic, A. Radenovic, J. Brivio, V. Giacometti and A. Kis, *Nat. Nanotechnol.*, 2011, **6**, 147-150.

15 H. Liu, J. Gu and P. D. Ye, *Ieee Electr. Device Lett.*, 2012, **33**, 1273-1275.

16 Z. Li, X. Li and J. Yang, *ACS Appl. Mater. Interfaces*, 2015, **7**, 12981-12987.
17 H. L. Zeng, J. F. Dai, W. Yao, D. Xiao and X. D. Cui, *Nat. Nanotechnol.*, 2012, **7**, 490-493.
18 S. Zhang, Z. Yan, Y. Li, Z. Chen and H. Zeng, *Angew. Chem. Int. Ed.*, 2015, **54**, 3112-3115.
19 C. Kamal and M. Ezawa, *Phys. Rev. B*, 2015, **91**, 085423.
20 L. Kou, Y. Ma, X. Tan, T. Frauenheim, A. Du and S. Smith, *J. Phys. Chem. C*, 2015, **119**, 6918-6922.
21 Y. Wang and Y. Ding, *Nanoscale Res. Lett.*, 2015, **10**, 955-955.
22 Y. Wang and Y. Ding, *J. Phys.: Condens. Matter*, 2015, **27**, 225304-225314.
23 S. Zhang, Y. Hu, Z. Hu, B. Cai and H. Zeng, *Appl. Phy. Lett.*, 2015, **107**, 022102.
24 Y. H. Hu, S. L. Zhang, S. F. Sun, M. Q. Xie, B. Cai and H. B. Zeng, *Appl. Phy. Lett.*, 2015, **107**, 122107.
25 K. Dolui, I. Rungger, C. Das Pemmaraju and S. Sanvito, *Phys. Rev. B*, 2013, **88**, 075420.
26 A. Ramasubramaniam and D. Naveh, *Phys. Rev. B*, 2013, **87**, 195201.
27 J. S. Qi, X. Li, X. F. Chen and K. G. Hu, *J. Phys.: Condens. Matter*, 2014, **26**, 256003.
28 X. X. Li, J. Zhao and J. L. Yang, *Sci. Rep.*, 2013, **3**, 1858.
29 Y. G. Zhou, J. Xiao-Dong, Z. G. Wang, H. Y. Xiao, F. Gao and X. T. Zu, *Phys. Chem. Chem. Phys.*, 2010, **12**, 7588-7592.
30 W. Fang, K. Erjun, X. Hongjun, W. Su-Huai, W. Myung-Hwan and Y. Jinlong, *Appl. Phy. Lett.*, 2009, **94**, 223105.
31 L. B. Luo, X. B. Yang, F. X. Liang, J. S. Jie, C. Y. Wu, L. Wang, Y. Q. Yu and Z. F. Zhu, *J. Phys. Chem. C*, 2011, **115**, 24293-24299.
32 L. B. Luo, X. B. Yang, F. X. Liang, J. S. Jie, Q. Li, Z. F. Zhu, C. Y. Wu, Y. Q. Yu and L. Wang, *Crystengcomm*, 2012, **14**, 1942-1947.
33 P. E. Blochl, *Phys. Rev. B: Condens. Matter Mater. Phys.*, 1994, **50**, 17953-17979.
34 G. Kresse and J. Furthmuller, *Comput. Mater. Sci.*, 1996, **6**, 15-50.
35 G. Kresse and D. Joubert, *Phys. Rev. B: Condens. Matter Mater. Phys.*, 1999, **59**, 1758-1775.
36 J. P. Perdew, K. Burke and M. Ernzerhof, *Phys. Rev. Lett.*, 1996, **77**, 3865-3868.
37 G. A. Henkelman, A; Jonsson, H, *Comput. Mater. Sci.*, 2006, **36**, 354-360.